

ELOVL2 controls the level of n-6 28:5 and 30:5 fatty acids in testis, a prerequisite for male fertility and sperm maturation in mice

Damir Zdravec,* Petr Tvrđik,[†] Hervé Guillou,[§] Richard Haslam,** Tsutomu Kobayashi,* Johnathan A. Napier,** Mario R. Capecchi,[†] and Anders Jacobsson^{1,*}

The Wenner-Gren Institute,* Arrhenius Laboratories F3, Stockholm University, Stockholm, Sweden; Howard Hughes Medical Institute,[†] University of Utah, Salt Lake City, UT; Laboratoire de Pharmacologie et Toxicologie,[§] Institut National de la Recherche Agronomique, Toulouse, France; and Department of Biological Chemistry,** Rothamsted Research, Harpenden, United Kingdom

Abstract ELOVL2 is a member of the mammalian microsomal ELOVL fatty acid enzyme family, involved in the elongation of very long-chain fatty acids including PUFAs required for various cellular functions in mammals. Here, we used ELOVL2-ablated (*Elovl2*^{-/-}) mice to show that the PUFAs with 24–30 carbon atoms of the ω-6 family in testis are indispensable for normal sperm formation and fertility in male mice. The lack of *Elovl2* was associated with a complete arrest of spermatogenesis, with seminiferous tubules displaying only spermatogonia and primary spermatocytes without further germinal cells. Furthermore, based on acyl-CoA profiling, heterozygous *Elovl2*^{+/-} male mice exhibited haploinsufficiency, with reduced levels of C28:5 and C30:5n-6 PUFAs, which gave rise to impaired formation and function of haploid spermatides. These new insights reveal a novel mechanism involving ELOVL2-derived PUFAs in mammals and previously unrecognized roles for C28 and C30 n-6 PUFAs in male fertility. In accordance with the function suggested for ELOVL2, the *Elovl2*^{-/-} mice show distorted levels of serum C20 and C22 PUFAs from both the n-3 and the n-6 series. However, dietary supplementation with C22:6n-3 could not restore male fertility to *Elovl2*^{+/-} mice, suggesting that the changes in n-6 fatty acid composition seen in the testis of the *Elovl2*^{+/-} mice, cannot be compensated by increased C22:6n-3 content.—Zdravec, D., P. Tvrđik, H. Guillou, R. Haslam, T. Kobayashi, J. A. Napier, M. R. Capecchi, and A. Jacobsson. **ELOVL2 controls the level of n-6 28:5 and 30:5 fatty acids in testis, a prerequisite for male fertility and sperm maturation in mice.** *J. Lipid Res.* 2011. 52: 245–255.

Supplementary key words fatty acid elongase • omega-6 • spermatogenesis

This work was supported by grants from the Swedish Research Council and Cancer Foundation (A.J.), Sven och Dagmar Saléns stiftelse (D.Z.), Institut National de la Recherche Agronomique, and Formas (H.G. and A.J.). Rothamsted Research receives grant support from the Biotechnology and Biological Sciences Research Council, United Kingdom (J.N.).

Manuscript received 16 September 2010 and in revised form 19 November 2010.

Published, JLR Papers in Press, November 24, 2010

DOI 10.1194/jlr.M011346

Copyright © 2011 by the American Society for Biochemistry and Molecular Biology, Inc.

This article is available online at <http://www.jlr.org>

Essential fatty acids, i.e., linoleic (C18:2n-6) and α-linolenic acid (C18:3n-3), which are prerequisites for normal growth, development, and function in mammals, cannot be synthesized de novo and, as such, have to be derived from diet (1). Subsequently, the C18:2n-6 and C18:3n-3 fatty acids can be converted into other PUFAs through a series of elongation and desaturation steps performed by distinct enzymes residing in the endoplasmic reticulum (2). Desaturation steps are performed by the Δ5- and Δ6-desaturases, while chain elongation is controlled by the elongation of very-long-chain fatty acid (ELOVL) enzymes, ELOVL2, ELOVL4, and ELOVL5. ELOVL4 is believed to be involved in the elongation of PUFAs in the retina, brain, skin, and testis (3). Using cultured cells that overexpress this protein, it has been shown that ELOVL4 is involved in the synthesis of saturated C28 and C30 very-long-chain FA (VLCFA), as well as polyunsaturated C28–C38 VLC-PUFAs such as the C34:6n-3 and C36:6n-3 fatty acids (4). ELOVL5 predominantly elongates C18 PUFAs up to 22 carbons in length, while ELOVL2 has been shown to be involved in the elongation of C20 and C22 PUFA in order to produce C24:4n-6 and C24:5n-3 PUFAs (5–7). These latter two are also recognized as precursors for docosapentaenoic acid (C22:5n-6) and docosahexaenoic acid (DHA) (C22:6n-3) synthesis, respectively, via the so-called Sprecher pathway, which includes one step of β oxidation/chain shortening (8).

To assess the in vivo function of ELOVL2, we generated *Elovl2*^{+/-} and *Elovl2*^{-/-} mice by homologous recombination

Abbreviations: DHA, docosahexaenoic acid; dNTP, deoxynucleoside triphosphate; ELOVL, elongation of very-long-chain fatty acid (protein); ES, embryonic stem (cells); FAME, fatty acid methyl ester; Hz, heterozygous; KO, knockout; TK, thymidine kinase; VLCFA, very-long-chain FA.

To whom correspondence should be addressed.
e-mail: anders.jacobsson@wgi.su.se

and present evidence that ELOVL2 is essential for the formation of C24:5n-6 to C30:5n-6 PUFAs in testis and that these fatty acids are indispensable for normal spermatogenesis and fertility.

EXPERIMENTAL PROCEDURES

Elovl2 gene targeting

Genomic liver DNA from the 129/Sv mouse strain was used to isolate the *Elovl2* gene. A 4.8 kb fragment excised with *XhoI* and a 3.3 kb fragment excised with *SpeI* and *HindIII* was used for the targeting construct (Fig. 1A). A 2.4 kb neomycin resistance (*neo^r*) gene fragment was inserted into the construct using *SaII*, and a thymidine kinase (TK) cassette was inserted using a *SpeI* site at the 3' end of the *Elovl2* targeting construct. The targeting construct was linearized with *NruI* and electroporated into R1 embryonic stem (ES) cells derived from male 129/Sv agouti mice (9). ES

cells were cultured and subjected to positive/negative selection using G418 and fialuridine, (FIUA) respectively, and were further analyzed by Southern blotting (see below). The *Elovl2*-ablated ES cells were injected into C57BL/6J blastocysts, which were implanted into foster mothers (F₁, CBA x C57/BL6) according to standard procedures. Male offspring, being the most chimeric, were bred with C57BL/6J females to generate offspring heterozygous for the mutation.

Southern blot analysis

A 1.5 kb fragment at the 5' end of the targeting construct was used as a probe to confirm *Elovl2* disruption in ES cell clones and mouse tail DNA. The probe was labeled with α -dCTP (Amersham Bioscience), using Ready-To-Go DNA labeling beads (GE Healthcare) for >45 min at 37°C. Probes were purified with a Sephadex G-50 DNA-grade nick column (GE Healthcare) and subsequently denatured. In addition, the *neo^r* fragment was also used as a probe to confirm a specific targeting event. Approximately 10 μ g of ES cell DNA or mouse tail DNA was digested

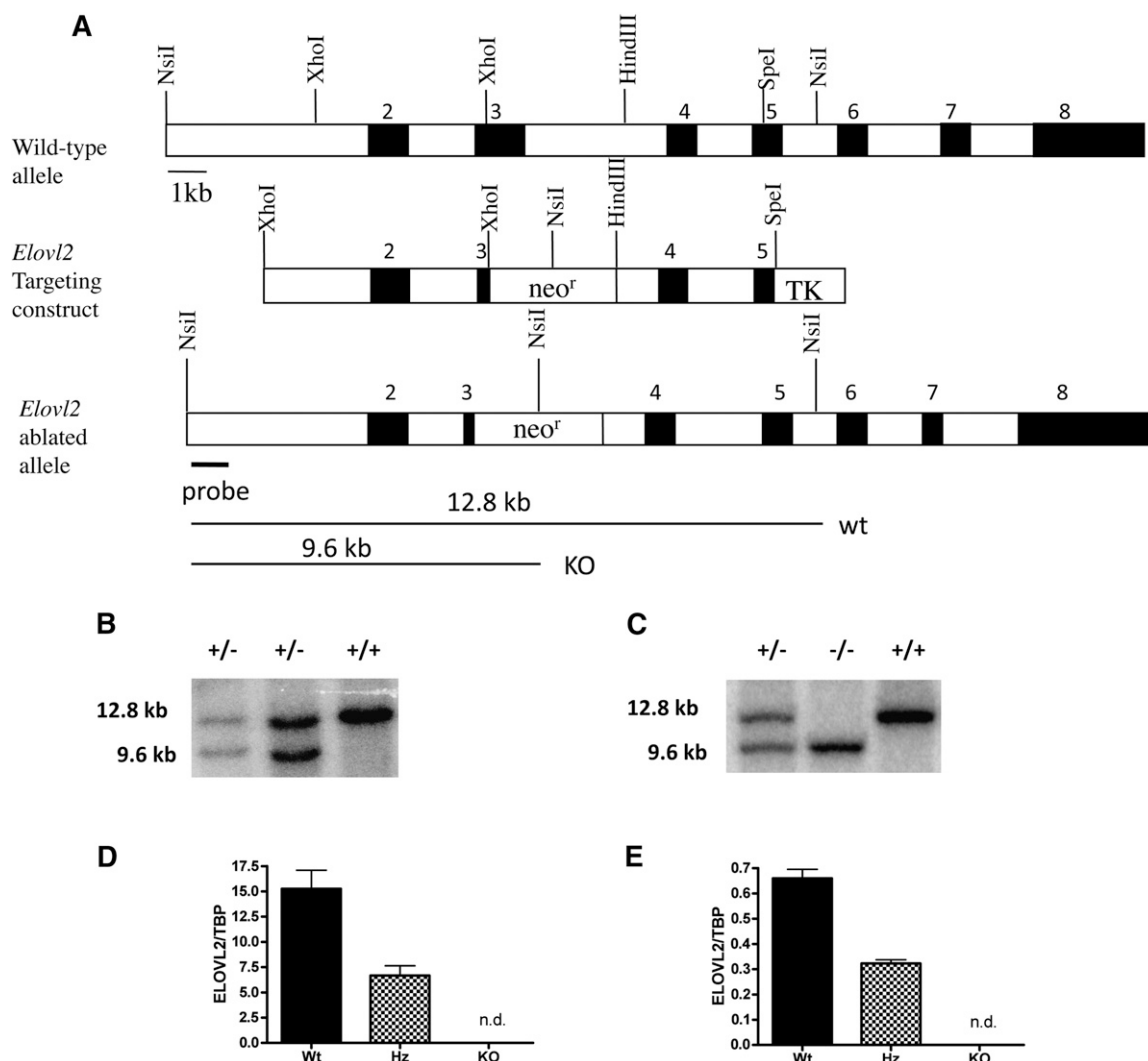


Fig. 1. Generation of *Elovl2*-ablated mice. **A:** *Elovl2* gene targeting construct. The neomycin resistance (*neo^r*) gene was used to replace a major portion of exon 3 in the ELOVL2 gene. The mutated *Elovl2* allele differs from that of the wild-type by the addition of an internal *NsiI* site in the *neo^r* gene. Black boxes represent exons and are numbered (2–8) above. TK, thymidine kinase. Genomic DNA from embryonic stem cells (**B**) and tail DNA (**C**) was digested with *NsiI* and analyzed with Southern blotting for the targeted *Elovl2* allele. Digestion yielded the 12.8 kb wild-type band and the 9.6 kb targeted band detected by the probe indicated in panel A. *Elovl2* expression analysis using real-time PCR is shown in liver (**D**) and testis (**E**). Results are means \pm SEM of 7 wild-type (Wt) heterozygous (Hz) mice and 2 knockout (KO) animals. *, $P < 0.05$; **, $P < 0.01$.

with *Nsi*I and separated using 1% agarose gel electrophoresis. DNA was denatured in a solution containing 0.2 M NaOH, 0.6 M NaCl for 30 min and in a solution of 0.5 M Tris (pH 7.5), 1.5 M NaCl for 30 min. Digested DNA was transferred to Hybond-XL membrane (Amersham Bioscience) in 20× SSC (1× SSC is 0.15 M NaCl plus 0.015 M sodium citrate) overnight and cross-linked to the membrane using a UV Stratalinker 1800 unit (Stratagene). Membranes were prehybridized in a solution of 50% formamide, 5× SSC, 5× Denhart's solution, 50 mM sodium phosphate, 0.5% SDS, and 1.5 mg of degraded herring sperm DNA (Sigma Aldrich) at 42°C. After membranes were prehybridized, they were transferred to a similar solution containing the denatured probe. Hybridization was carried out at 42°C overnight. Membranes were washed in a mixture of 2× SSC, 0.2% SDS at room temperature for 15 min and in 0.1× SSC, 0.2% SDS at 43°C for 15 min and analyzed by phosphorimaging using an FLA-3000 reader (Fuji).

Animals

All animals were housed at 22°C and maintained on a 12 h light:12 h dark cycle. Animals were fed ad libitum with Rat and Mouse standard chow (no.1; BeeKay Feeds, B and K Universal, Stockholm, Sweden) and had free access to water. All studies were carried out with permission from the Animal Ethics Board in Stockholm, Sweden.

Dietary supplementation

Male and female *Elovl2*^{+/-} mice were fed a DHA (C22:6n-3)-enriched diet (19.5% of total) obtained from Polaris (Quimper, France), for 3 months ad libitum. For the fatty acid composition of the diet see Table 3.

Quantitative RT-PCR

RNA was isolated with Ultraspec RNA isolation solution (Bio-site, San Diego, CA), and total RNA was isolated according to the manufacturer's procedure. For real-time PCR, 500 ng of total RNA was reverse transcribed using random hexamer primers, deoxynucleoside triphosphates (dNTPs), multiscript, and RNase inhibitor (Applied Biosystems, Foster City, CA). Complementary DNA samples were diluted 1:10, and 2 μl aliquots of sample cDNA were mixed with SYBR Green JumpStart *Taq* ReadyMix (Sigma Aldrich), prevalidated primers, and diethyl pyrocarbonate DEPC, Sigma)-treated water and measured in duplicate for each sample. Expression analysis was performed with an ABI Prism 7000 sequence detection system (Applied Biosystems). Data were normalized to TFIIb or TBP.

MRI measurement

In vivo MRI using an EchoMRI-100™ machine (Echo Medical Systems, Houston, TX) was performed in order to measure body fat and lean contents.

Lipid profiling

Triglyceride and fatty acid assays were performed as previously described (10). To measure total fatty acid methyl ester (FAME) molecular species, lipid amounts corresponding to an equivalent of 3 mg of tissue were extracted in the presence of glyceryl triheptadecanoate (0.5 μg) as an internal standard. Lipid extract was transmethylated with 1 ml of BF₃ in methanol (1/20, v/v) for 150 min at 100°C and evaporated to dryness, and the FAME species were extracted with hexane-water, 1:1. The organic phase was evaporated to dryness and dissolved in 50 μl of ethyl acetate. One microliter of FAME was analyzed by gas-liquid chromatography using a 5890 Hewlett Packard system with Restek Famewax fused silica capillary columns (30 m × 0.32 mm ID; 0.25 mm film

thickness). Oven temperature changes were programmed from 110°C to 220°C at a rate of 2°C per min, and the carrier gas was helium (0.5 bar). Injector and detector temperatures were 225°C and 245°C, respectively.

HPLC Analysis of acyl-etheno-CoA derivatives

Twenty milligram portions of material were frozen in liquid nitrogen and subsequently extracted for quantitative analysis of fluorescent acyl-etheno-CoA derivatives by HPLC. Analysis of acyl-CoA was performed using an Agilent 1100 LC system (LUNA 150 × 3.2 mm C18[2] column; Phenomenex); methodology and gradient conditions have been described previously (11–13).

Histology

At necropsy, testis and epididymis tissues were fixed in 10% neutral buffered formalin, sectioned, stained with hematoxylin and eosin, and examined by light microscopy for histological evaluation.

RESULTS

ELOVL2 expression is critical for normal male fertility

Real-time quantitative PCR revealed a reduction of almost exactly 50% of *Elovl2* mRNA transcript in the liver and testis of the *Elovl2*^{+/-} mice (Fig. 1D, E), indicating an *Elovl2* haploinsufficiency in these mice. No transcript was found in the *Elovl2*^{-/-} mice. Breeding of *Elovl2*^{+/-} mice for further production of *Elovl2*^{-/-} mice displayed severe fertility problems, as shown by reduced production of offspring.

Elovl2^{+/-} female and *Elovl2*^{+/+} male mice gave rise to offspring of both the *Elovl2*^{+/+} and the *Elovl2*^{+/-} genotypes in a normal ratio, while 90% of all *Elovl2*^{+/-} males tested (36/40) were shown to be infertile during their reproductive period (1 year), and only 2 of the fertile males gave rise to more than one litter. In addition, heterozygous breeding did not produce offspring in a normal 1:2:1 Mendelian ratio. Rather, the ratio between *Elovl2*^{+/+} and *Elovl2*^{+/-} genotypes was close to 1:1, and of about 300 offspring, only 3 *Elovl2*^{-/-} mice (2 males and 1 female) were born. As no indications of embryonic lethality were observed, this implies a deficiency of spermatogenesis in *Elovl2*^{+/-} mice. The two male *Elovl2*^{-/-} mice were both sterile, while the female mouse was able to produce offspring together with wild-type males.

No differences were seen in body weight, fat and lean contents, or liver weight among the wild-type, *Elovl2*^{+/-}, and *Elovl2*^{-/-} male mice fed on a standard chow diet (Table 1). However, the two male *Elovl2*^{-/-} mice exhibited marked hypogonadism, with testis weight reduced by 60% compared with age-matched controls.

ELOVL2 is essential for normal spermatogenesis

Histological analyses of wild-type testis showed all stages of spermatogenesis (Fig. 2A–C), and mature spermatozoa were elongated and displayed a marked hook-shaped head (Fig. 2C, arrow). In contrast, seminiferous tubules of the *Elovl2*^{-/-} mice displayed spermatogonia with numerous mitoses and primary spermatocytes but lacked further germinal cells (Fig. 2I–L). The primary spermatocytes degenerated and formed multinucleate giant cells that desquamated in the lumen of the seminiferous tubule with

TABLE 1. Phenotypic comparison of wild-type, *Elovl2*^{+/-}, and *Elovl2*^{-/-} male mice

Parameter	<i>Elovl2</i> ^{+/+}	<i>Elovl2</i> ^{+/-}	<i>Elovl2</i> ^{+/+}	<i>Elovl2</i> ^{-/-}
Sex	Male	Male	Male	Male
Age (weeks)	14	14	22/52	22/52
Number of mice	7	6	2	2
Body weight (g)	30.7 ± 0.8	30.4 ± 0.7	40.6 ± 0.9	42.5 ± 6.1
Fat content (g)	4.4 ± 0.8	4.4 ± 0.4	11.7 ± 1.0	12.2 ± 4.1
Lean content (g)	23.6 ± 0.4	23.1 ± 0.5	25.4 ± 0.1	25.4 ± 1.6
Liver weight (g)	1.5 ± 0.1	1.4 ± 0.1	NA	NA
Testis weight (g)	0.22 ± 0.01	0.23 ± 0.01	0.25 ± 0.01	0.10 ± 0.02

Characteristics of mice at 14 weeks of age (*Elovl2*^{+/+} and *Elovl2*^{+/-}) or at 22 and 52 weeks of age (*Elovl2*^{+/+} and *Elovl2*^{-/-}, respectively) fed on standard chow diet. Results shown are means ± SEM. NA, not analyzed

an incomplete formation of the four haploid spermatids (Fig. 2K, L, arrows). These changes were observed in every section of seminiferous tubules of both testicles and were consistent with bilateral testicular hypoplasia and arrested spermatogenesis; however, both the Sertoli cells and the Leydig cells appeared normal in the interstitium.

Testis of the *Elovl2*^{+/-} male mice showed normal seminiferous tubules displaying normal Sertoli cells, and the Leydig cells in the interstitium were normal; however, heterozygote mice displayed abnormal sperm morphology, with numerous spermatozoa displaying a rounded, condensed head (Fig. 2E–G), and the condensed nucleus frequently displayed a small rounded vacuole measuring about 1–2 μm (Fig. 2G, arrowhead). Nonetheless, sperm were subsequently released into the lumen and attained normal flagellar movement. The epididymis of the *Elovl2*^{+/-} mice showed the presence of numerous spermatozoa, which, as in the seminiferous tubules, displayed rounded and condensed heads (Fig. 2H). No obvious differences were noticed in total number of sperm, which is in line with the normal testis weight found in heterozygote mice. Together, these data show that the impaired fertility in *Elovl2*^{+/-} and *Elovl2*^{-/-} male mice is due to developmental blockage of spermatide formation and occurs at the stage of sperm head packaging during spermatogenesis, respectively (Fig. 2M).

Gene expression of spermatogenesis markers

As expected, the levels of mRNA expression of several stage-specific gene products, which are controlled by the bZip-type cAMP-responsive element modulator (CREM) transcription factor during late spermiogenesis (14), were dramatically downregulated in the *Elovl2*^{-/-} mice, including the A-kinase anchoring protein-3 (AKAP3), a scaffolding protein for regulatory proteins in the flagella; transcript induced in spermiogenesis 50 (TISP50), a sperm flagellar protein; TISP69, an E3 ligase promoting proteasome-mediated degradation of spermatid proteins in the late spermatid stage; and transition protein-1 (Tnp1), which is involved in sperm head compaction (Fig. 3A–D). However, the expression levels of these same encoding genes were unchanged in the *Elovl2*^{+/-} mice, which is consistent with the fact that it is the formation and extrusion of the head components of the spermatids during their release into the lumen of the seminiferous tubules and not the formation of the flagellum and mitochondrial sheath that is impaired

in the heterozygote *Elovl2*^{+/-} mice. Of the genes investigated, only the *Cttn* (cortactin) gene expression, which is expressed in the apical membrane of Sertoli cells facing germ cells and is involved in a complex of spermatid-Sertoli cell interactions during spermatid head shaping (15, 16), was changed in *Elovl2*^{+/-} male mice (Fig. 3E).

ELOVL2 controls the synthesis of 28:5 and 30:5n-6 PUFA in testis

In order to directly link PUFA synthesis in the testis with the impaired spermatogenesis seen in our mutant mice, acyl-CoA profiling of testis was performed in the *Elovl2*^{-/-} and *Elovl2*^{+/-} mice and compared with that in age-matched littermates. When we looked at the metabolic pool in which the *Elovl* enzymes work, except for the C22:6n-3 (DHA) PUFA, the levels of n-3 PUFA-CoAs were too low to be identified within the testis; however, the *Elovl2*^{-/-} mice exhibited increased levels of C22:4n-6-CoA, accompanied by significantly reduced levels of C22:5n-6-CoA (Fig. 4A). Intriguingly, the mice exhibited an almost complete loss of the acyl-CoA elongation products of C24:5n-6, that is, C26:5n-6, C28:5n-6, and C30:5n-6. These results describe a novel role for ELOVL2 in the formation of VLC-PUFAs and show that n-6 PUFA elongation beyond 22:4 in testis is exclusively dependent on ELOVL2 activity (Fig. 5, gray area).

To further assess the consequences of impaired *Elovl2* expression in the heterozygote mice, it was clearly shown that as in *Elovl2*^{-/-} mice, the acyl-CoA levels of C28:5n-6 and C30:5n-6 PUFA were significantly reduced in the testis of *Elovl2*^{+/-} mice as well (Fig. 4B). In addition to the changes observed in PUFA levels, we noted a decrease in total fatty acids (FAME mass) and triglycerides in the *Elovl2*^{+/-} mice (Table 2). Despite this, there were no differences in the composition of triacylglycerols among the mouse strains. The levels of cholesterol, which is the substrate for testosterone synthesis in Leydig cells, and cholesterol esters were not different between wild-type and *Elovl2*^{+/-} mice (Table 2), indicating that testosterone production is normal in the *Elovl2*^{+/-} mice. In addition, there were no differences in the appearance of the vesicula seminalis, again, implying that the androgen levels are normal in the *Elovl2*^{+/-} mice.

Because *Elovl2* expression was reduced in the liver of heterozygote *Elovl2*^{+/-} male mice to a level that was similar to that in testis, we also performed total lipid profiling by gas chromatography analysis of liver fatty acids and compared those results with levels in testis. Although we were unable to detect any fatty acids longer than C24 in liver, no major changes were seen in PUFA levels in *Elovl2*^{+/-} mice (Fig. 6A). However, in testis, the level of C20:4n-6 was increased to 25% of total fatty acids compared with that in wild-type mice testis (Fig. 6B), implying a differential mechanism in the control of PUFA levels in different tissues. Furthermore, the elongated product of C20:4n-6 (i.e., C22:4n-6) was increased by almost 70%. Surprisingly, in contrast to the *Elovl2*^{-/-} mice (Fig. 6C), no reduction was seen in the levels of C22:5n-6 and C22:6n-3, suggesting that the activity of Δ6-desaturase is very sensitive to the levels of these fatty acids in testis.

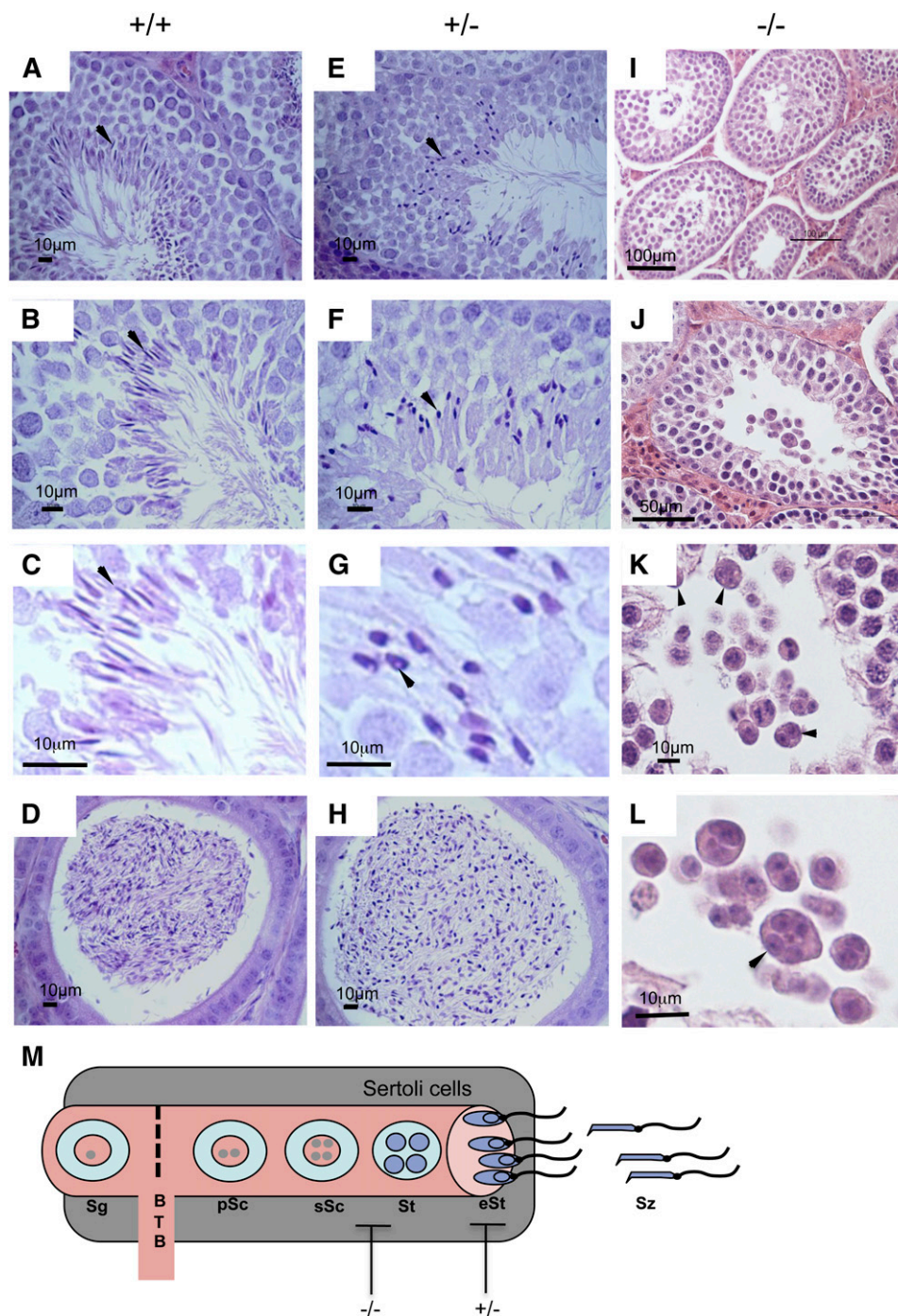


Fig. 2. Histological analysis of testes in wild-type, *Elov12*^{+/-}, and *Elov12*^{-/-} mice. Mature spermatozoa are shown with elongated heads in seminiferous tubules (A–C, arrows) and epididymes (D) of wild-type mice. *Elov12*^{+/-} testis are seen with numerous spermatozoa displaying rounded, condensed heads (E–G, arrows), and the condensed nucleus frequently displays a small rounded vacuole about 1–2 μm (G, arrowhead). Epididymes of wild-type (D) and *Elov12*^{+/-} (H) mice display spermatozoa with rounded heads compared with those of wild-type epididymis. *Elov12*^{-/-} mice displayed only spermatogonia and primary spermatocytes (I, J) with multinucleate giant cells in the lumen (K, L, arrows). (M) Spermatogenesis within the seminiferous tubules and blockage by *Elov12* ablation in *Elov12*^{-/-} and *Elov12*^{+/-} mice. Sg, spermatogonia; pSc, primary spermatocytes; sSc, secondary spermatocytes; BTB, blood testis barrier; St, spermatides; eSt, elongated spermatides; Sz, spermatozoa.

Deficiencies in serum levels of n-3 and n-6 fatty acids in *Elov12*^{-/-} mice

When we analyzed serum lipid composition, we found that C20:5n-3 and C22:5n-3 levels in *Elov12*^{-/-} mice were increased compared with that in age-matched littermates

(Fig. 7), which suggests that *Elov12* ablation causes a general blockage in the elongation of C22:5n-3 for the formation of C24:5n-3, which is the substrate for $\Delta 6$ -desaturase and precursor for C22:6n-3 synthesis (Fig. 5). In addition, finding that the level of C22:5n-6, which is the final product

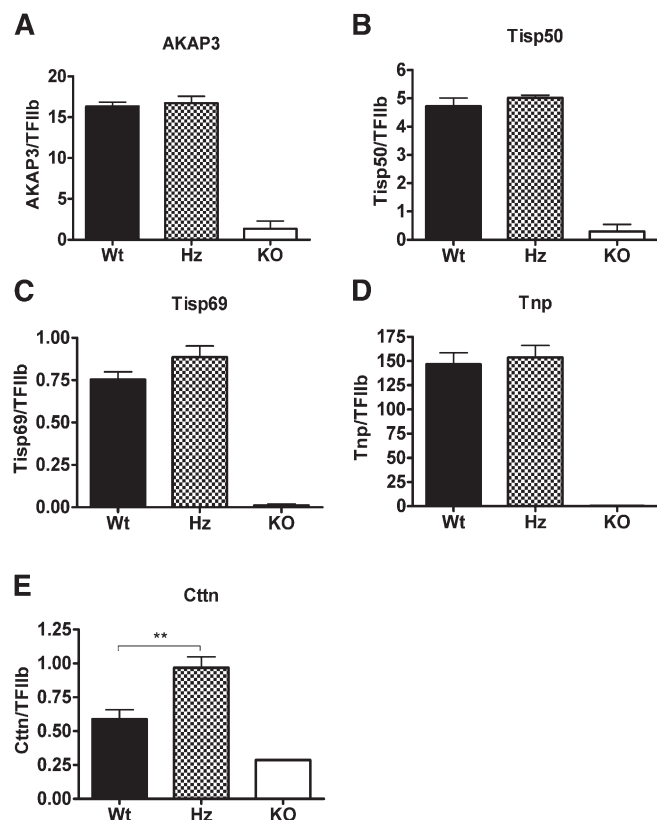


Fig. 3. Testicular gene expression. Analysis of the *AKAP3* (A), *TISP50* (B), *TISP69* (C), *Tnp* (D) and *Ctn* (E) genes were examined by real-time PCR in wild-type (Wt), *Elovl2*^{+/-} (Hz [heterozygous]), and *Elovl2*^{-/-} (KO [knockout]) mice. Results shown are the means \pm SEM of 7 Wt and Hz animals and 2 KO animals. *, $P < 0.05$; **, $P < 0.01$.

of C22:4n-6 elongation and $\Delta 6$ -desaturation, also was reduced implies that ELOVL2 is important for C22 elongation within both the n-3 and the n-6 series (Fig. 5).

DHA supplementation does not restore fertility in male *Elovl2*^{+/-} mice

Recently, two different mouse strains lacking $\Delta 6$ -desaturase (*FADS2*) have been associated with impaired reproduction. As in the case of *Elovl2*^{+/-} mice, *Fads2*-ablated mice show abnormal sperm head conformation (17, 18) and are characterized by a reduction in levels of C20:4n-6, C22:5n-6, and C22:6n-3. Interestingly, dietary supplementation of C22:6 n-3 (DHA) completely restored sperm morphology and subsequently male fertility of these mice (19), suggesting that 22:5n-6 PUFA are dispensable if 22:6n-3 is supplemented in the diet. In contrast, despite distorted levels of C22 PUFAs in testis of *Elovl2*^{+/-} mice, dietary supplementation of DHA for 3 months (Tables 3 and 4) could not restore male fertility of these mice, emphasizing the importance of ELOVL2 and the generation of testis-specific VLC-PUFA required for male fertility.

DISCUSSION

Here we report a novel mechanism involving ELOVL2-derived fatty acids in mammalian spermatogenesis. Using homologous recombination, we developed *Elovl2*^{-/-} mice,

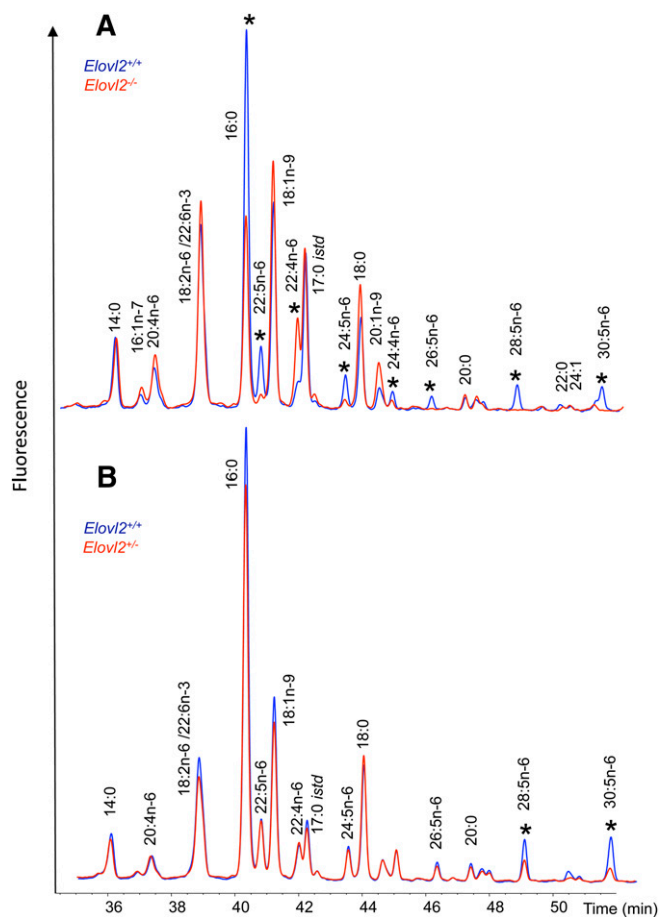


Fig. 4. Biosynthesis of VLC-PUFAs in wild-type, *Elovl2*^{+/-}, and *Elovl2*^{-/-} mice. The composition of the testicular acyl-CoA pool was determined by extraction, derivatization, and HPLC analysis of acyl-etheno-CoAs. Carbon 17:0 *istd* is the internal standard acyl-CoA. A: Acyl-CoA composition of wild-type and *Elovl2*^{-/-} testes. Blue trace corresponds to *Elovl2*^{+/-}, and the red trace corresponds to *Elovl2*^{-/-} mice. *, indicates differences between the genotypes. B: Acyl-CoA composition of wild-type and *Elovl2*^{-/-} testes. Blue trace corresponds to *Elovl2*^{+/-} mice, and the red trace corresponds to *Elovl2*^{-/-} mice. *, indicates differences between the genotypes. Results shown are pooled samples from 7 wild-type and heterozygous mice and 2 knockout animals.

which resulted in a complete arrest of spermatogenesis, with seminiferous tubules displaying only spermatogonia and primary spermatocytes, without further germinal cells in male mice. The main reason for this result is the complete absence of C24–C30 VLC-PUFAs of the n-6 family in the testis, of which C24:4 n-6 is essential for the production of C22:5 n-6. Even more surprising is that heterozygote *Elovl2*^{+/-} mice exhibited haploinsufficiency with reduced levels of n-6 C28:5 and C30:5 PUFAs, which gives rise to impaired packaging of haploid spermatides and infertility in almost all male mice, implying that even minor changes in *Elovl2* expression and testicular omega-6 PUFA content may have severe effects on male reproduction ability. This implies that C28–C30 n-6 PUFAs are formed by *Elovl2* and are crucial for normal spermatogenesis, although we cannot rule out the possibility that the effect seen in *Elovl2*^{-/-} mice at an earlier stage of spermatogenesis may be a direct

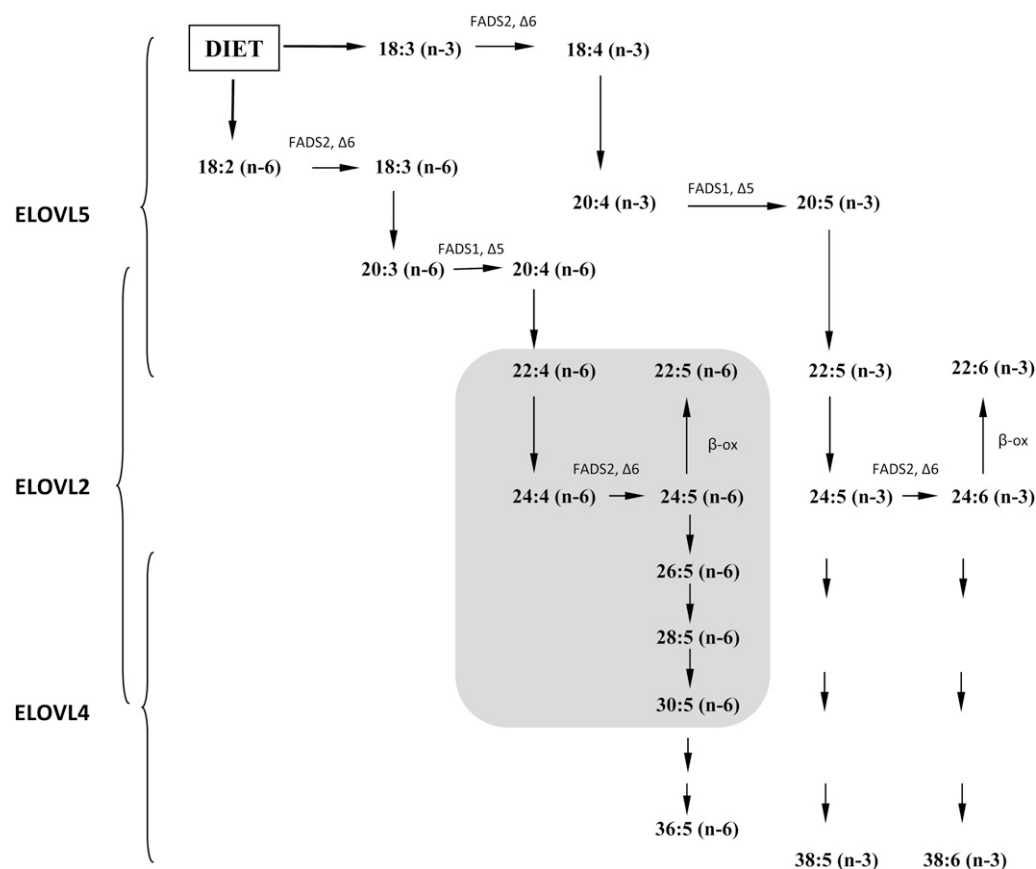


Fig. 5. In vivo VLC-PUFA biosynthesis by ELOVL2, ELOVL4, and ELOVL5. The 18:3n-3 and 18:2n-6 PUFAs were obtained from the diet and were subsequently elongated and desaturated by the indicated enzymes into longer PUFAs. ELOVL5 is involved in the elongation of PUFAs up to 22 carbons in length. ELOVL2 elongates from 20:4n-6 and 20:5n-3 series. Specifically, in the testis, ELOVL2 is involved in the biosynthesis of VLC-PUFA (\geq C24) up to 30 carbons in length of the n-6 family (gray area). ELOVL4 elongates up to C38 in length. C26FADS, fatty acid desaturase.

consequence of impaired levels of C22–C26 PUFAs as well.

The histological phenotype of the *Elovl2*^{-/-} mice testis resembles in part the morphology seen in two mouse strains with disruption of the epimorphin gene, a member of the SNARE family, which plays an essential role in membrane fusion at the terminal step of cytokinesis and vesicle fusion during exocytosis (20–22). As in the case of *Elovl2* ablation, those germ cells failed to complete the meiotic division to generate haploid cells, thereby resulting in the formation of multinucleated cells in the lumens of the seminiferous tubules. In addition, mutations within the *bond* gene, an *Elovl* homolog in *Drosophila*, with unknown fatty acid specificity, block cleavage-furrow ingression during early telophase in dividing spermatocytes, which is due to collapse of the contractile rings as a consequence of impaired interaction between cytoskeleton and plasma membrane at this stage (23). Those findings together with our data presented here imply that ELOVL2-synthesized VLC PUFAs are essential membrane components for normal completion of spermatocyte cytokinesis in mammals.

With maturation, the spermatides accumulate significant amounts of unusual sphingolipids containing VLC PUFAs (24, 25), which are principally localized to the sperm head

(26) where they may stabilize cellular membranes with high curvature, such as the rims of the sperm head. In addition, during acrosomal biogenesis, proacrosomal vesicles derived from the Golgi apparatus dock and fuse along a cytoskeletal plate, which then reorganizes to modulate exogenous shear forces exerted by the Sertoli cells to guide nuclear elongation

TABLE 2. Neutral lipid composition in testis of wild-type and *Elovl2*^{-/-} male mice

Lipid class and length	Wild-type mice	<i>Elovl2</i> ^{-/-} mice
Triglyceride C49	2.5 ± 0.9 ^a	3.5 ± 0.7
Triglyceride C51	5.5 ± 0.5 ^a	6.0 ± 0.6
Triglyceride C53	25.5 ± 0.9 ^a	25.6 ± 0.7
Triglyceride C55	38.8 ± 1.7 ^a	36.8 ± 1.4
Triglyceride C57	23.0 ± 0.7 ^a	22.5 ± 0.7
Triglyceride C59	4.7 ± 1.7 ^a	5.7 ± 1.2
Cholesterol	15.3 ± 0.9 ^b	13.5 ± 0.9
Cholesterol esters	2.7 ± 0.4 ^b	2.3 ± 0.3
Cholesterol esters C16	36.5 ± 2.0 ^a	37.2 ± 1.2
Cholesterol esters C18	55.1 ± 2.4 ^a	54.7 ± 1.2
Cholesterol esters C20:4 (n-6)	8.5 ± 1.7 ^a	8.1 ± 1.8
Triglycerides	32.4 ± 10.8 ^b	14.4 ± 5.4
Relative FAME mass	63.9 ± 11.7	22.0 ± 6.0 ^{**}

^a Units are percentage of total ± SEM.

^b Units are µg/mg.

^{**}, P < 0.01.

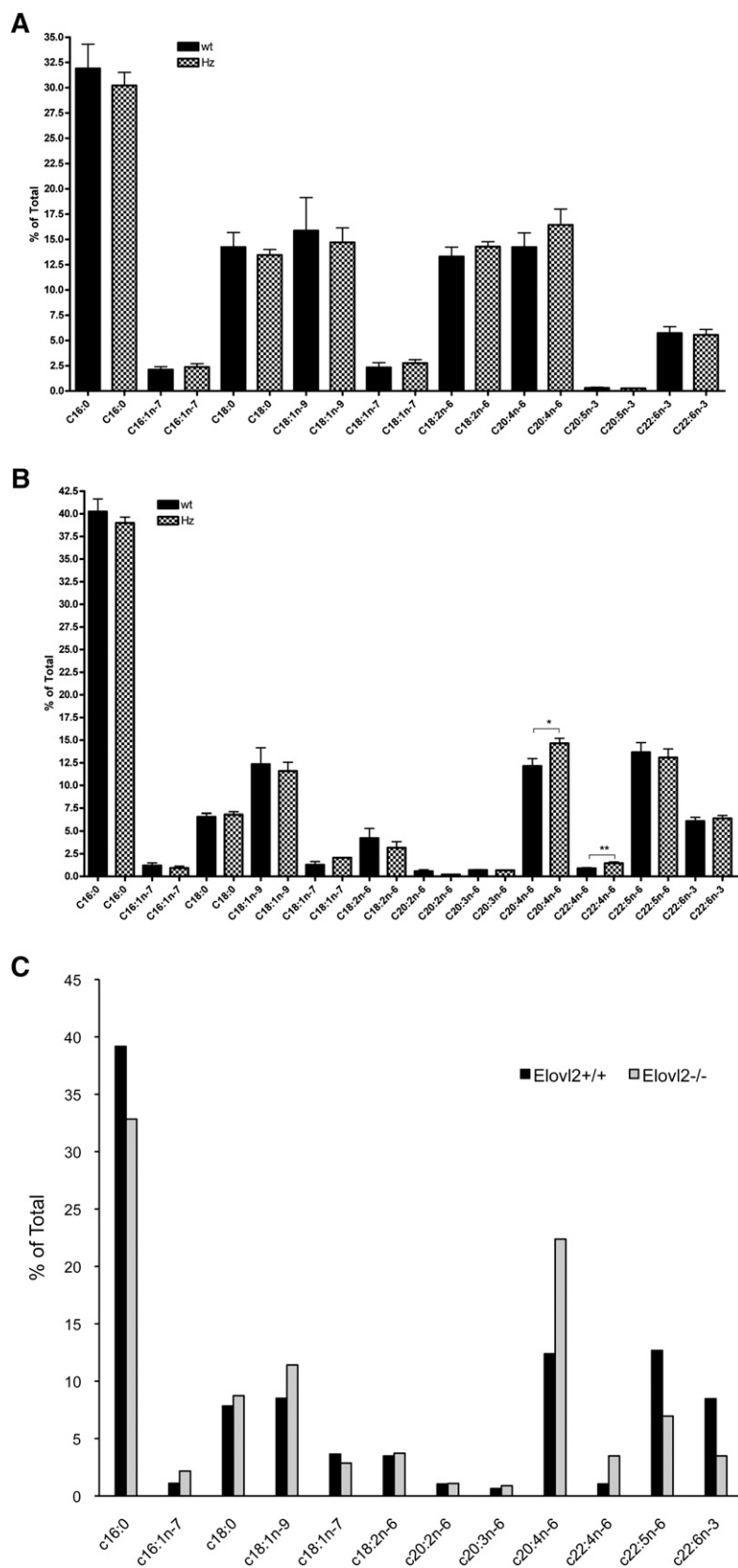


Fig. 6. Total fatty acid composition of liver and testis. Fatty acid composition up to C24, analyzed by gas chromatography of liver (A) and testis (B) of wild-type (wt) and *Elovl2*^{+/-} (Hz [heterozygous]) male mice and testis of two pooled wild-type and *Elovl2*^{-/-} male mice (C). Bars indicate means \pm SEM from 6 animals. *, $P < 0.05$; **, $P < 0.01$.

(27). Our data for heterozygote *Elovl2*^{+/-} mice imply that *Elovl2*-derived C28:5 and C30:5 n-6 fatty acids are essential membrane components in circumstances when exceptionally strong forces are applied to the cell.

A distinguishing feature between the *Elovl2*^{+/-} mice and the *Fads2*- and *Elovl5*-ablated mice (Fig. 5) is that fertility is already severely affected at a heterozygous stage in *Elovl2*^{+/-} male mice, suggesting a dominant neg-

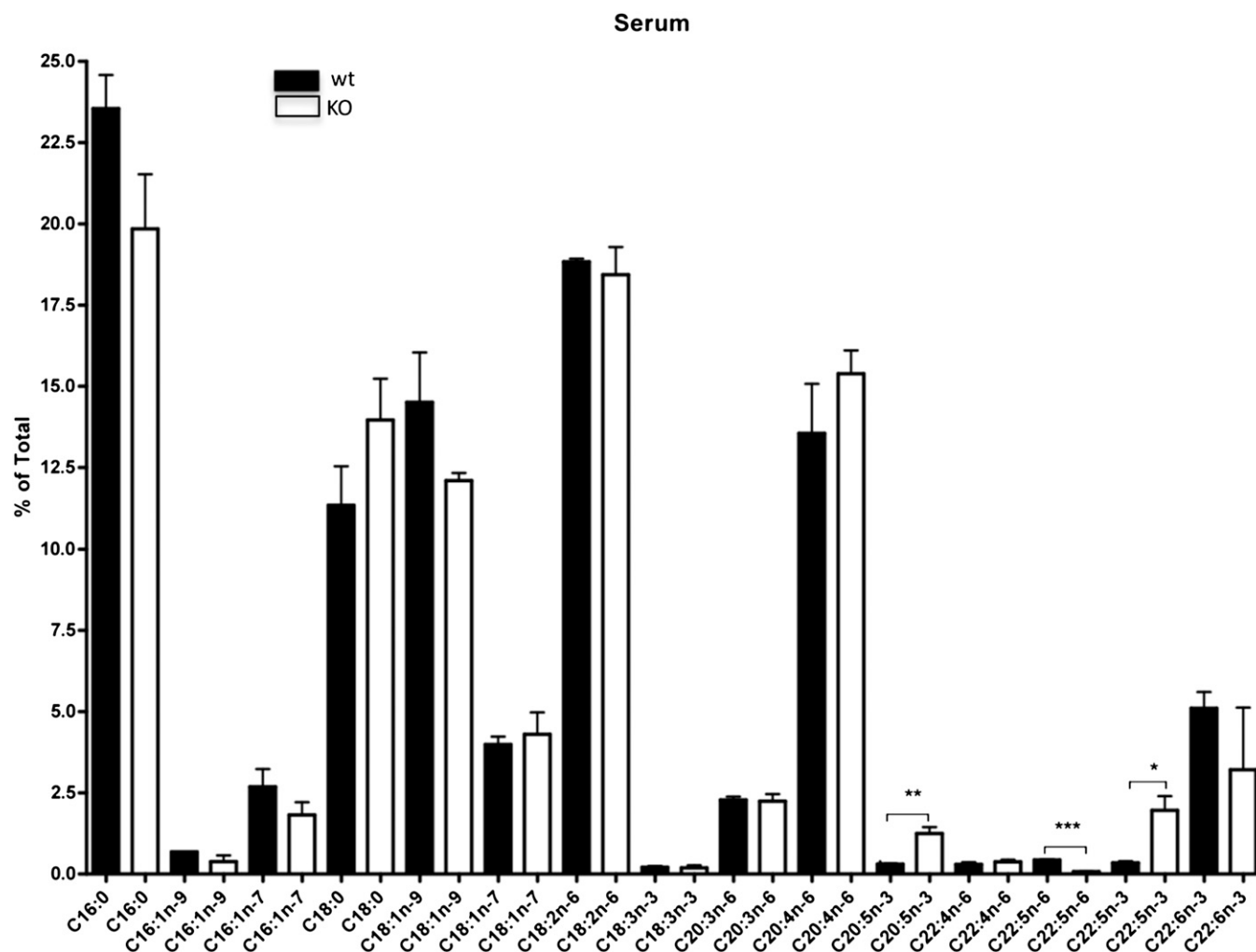


Fig. 7. Differences in total PUFA composition of serum. Fatty acid composition up to C24, by gas chromatography analysis of serum in wild-type and *Elov2*^{-/-} male mice. Bars indicate means \pm SEM from 3 animals per group. *, $P < 0.05$; **, $P < 0.01$; ***, $P < 0.001$.

ative effect, which cannot be rescued by any other metabolic pathway. In addition, mice heterozygous for both *Elov5* and *Fads2* ablation produce offspring in a normal Mendelian ratio, and male *Elov5*^{-/-} mice are fertile (18, 28).

Because ELOVL4 has been shown to be the enzyme responsible for VLC-PUFA synthesis in retina (3), the enzyme has been suggested to perform the same action in testis. As both ELOVL2 and ELOVL4 are expressed at significant levels in testis and retina, our data clearly imply that ELOVL2 and ELOVL4 have two distinct functions in these tissues: ELOVL2 preferentially elongates C22 PUFA up to C30 of the n-6 series, and ELOVL4 preferentially elongates C26 PUFA up to C36 of the n-3 series (Fig. 5). In addition, several mutations and deletions in the *Elov4* gene have been shown to be associated with the pathogenesis of dominant macular dystrophies in mice and humans (29–33). However, diabetes-induced retinopathy has recently been shown to be associated with reduced expression of both *Elov2* and *Elov4*, which is paralleled by a downregulation of DHA and n-3 VLC-PUFAs in retina (34), suggesting that ELOVL2 and ELOVL4 may operate at different levels also within the same elongation pathway.

It is noteworthy that in addition to its expression in retina and testis, *Elov4* is also expressed in skin (3). *Elov4*-ablated mice die within a few hours after birth due to dehydration caused by a reduction of specific ceramides and saturated VLCFA longer than C26 in the epidermis of mutant mice (35). In contrast, *Elov2* knockout mice do not show any obvious skin phenotype, which is in accordance with undetectable levels of *Elov2* expression in skin


TABLE 3. Fatty acid composition of DHA-enriched diet

Fatty acid	% of fatty acid in DHA diet
C12:0	0
C14:0	0
C16:0	4.44
C18:0	2.09
C18:1n-9	30.53
C18:2n-6	34.69
C18:3n-3	3.45
C20:5n-3	5.27
C22:6n-3	19.53
satfa	6.53
mufa	30.53
n-6	34.69
n-3	28.25

TABLE 4. DHA content in male liver after dietary supplementation

Measure	<i>Elovl2</i> ^{+/+} fed chow	<i>Elovl2</i> ^{+/-} fed chow	<i>Elovl2</i> ^{+/-} fed DHA supplement
% DHA ± SEM in liver	5.7 ± 0.6	5.5 ± 0.6	11.3 ± 3.5

of normal mice. Overall, these data emphasize ELOVL2 as the critical enzyme for the conversion of C22 to C26 PUFA, which may then act as a substrate for ELOVL4.

In summary, from our data here, it is apparent that de novo synthesis of n-6 VLC-PUFAs with C28 and C30 carbon atoms is a prerequisite of normal sperm maturation and that any interference with this process has severe consequences for male reproduction. Considering recent findings for the relationship between ELOVL2 expression and metabolic syndromes found in humans (36, 37), our results presented here may therefore give new insights into the field and show how nutritional interventions, and/or modulation of ELOVL2 expression, could represent a potential therapeutic target for male infertility caused by impaired lipid metabolism. 

The authors thank Dr. R. Feinstein, Dr. A. Asadi, Dr. O. Söder, B. Leksell, and S. Sundberg for technical assistance.

REFERENCES

- Burr, G. O., and M. M. Burr. 1973. Nutrition classics from The Journal of Biological Chemistry 82:345–67, 1929. A new deficiency disease produced by the rigid exclusion of fat from the diet. *Nutr. Rev.* **31**: 248–249.
- Guillou, H., D. Zdravec, P. G. Martin, and A. Jacobsson. 2010. The key roles of elongases and desaturases in mammalian fatty acid metabolism: Insights from transgenic mice. *Prog. Lipid Res.* **49**: 186–199.
- Mandal, M. N., R. Ambasudhan, P. W. Wong, P. J. Gage, P. A. Sieving, and R. Ayyagari. 2004. Characterization of mouse orthologue of ELOVL4: genomic organization and spatial and temporal expression. *Genomics*. **83**: 626–635.
- Agbaga, M. P., R. S. Brush, M. N. Mandal, K. Henry, M. H. Elliott, and R. E. Anderson. 2008. Role of Stargardt-3 macular dystrophy protein (ELOVL4) in the biosynthesis of very long chain fatty acids. *Proc. Natl. Acad. Sci. U.S.A.* **105**: 12843–12848.
- Leonard, A. E., E. G. Bobik, J. Dorado, P. E. Kroeger, L. T. Chuang, J. M. Thurmond, J. M. Parker-Barnes, T. Das, Y. S. Huang, and P. Mukerji. 2000. Cloning of a human cDNA encoding a novel enzyme involved in the elongation of long-chain polyunsaturated fatty acids. *Biochem. J.* **350**: 765–770.
- Moon, Y. A., N. A. Shah, S. Mohapatra, J. A. Warrington, and J. D. Horton. 2001. Identification of a mammalian long chain fatty acyl elongase regulated by sterol regulatory element-binding proteins. *J. Biol. Chem.* **276**: 45358–45366.
- Wang, Y., M. Torres-Gonzalez, S. Tripathy, D. Botolin, B. Christian, and D. B. Jump. 2008. Elevated hepatic fatty acid elongase-5 activity affects multiple pathways controlling hepatic lipid and carbohydrate composition. *J. Lipid Res.* **49**: 1538–1552.
- Sprecher, H. 2000. Metabolism of highly unsaturated n-3 and n-6 fatty acids. *Biochim. Biophys. Acta.* **1486**: 219–231.
- Nagy, A., J. Rossant, R. Nagy, W. Abramow-Newerly, and J. C. Roder. 1993. Derivation of completely cell culture-derived mice from early-passage embryonic stem cells. *Proc. Natl. Acad. Sci. U.S.A.* **90**: 8424–8428.
- Rebouissou, S., S. Imbeaud, C. Balabaud, V. Boulanger, J. Bertrand-Michel, F. Terce, C. Auffray, P. Bioulac-Sage, and J. Zucman-Rossi. 2007. HNF1alpha inactivation promotes lipogenesis in human hepatocellular adenoma independently of SREBP-1 and carbohy-

drate-response element-binding protein (ChREBP) activation. *J. Biol. Chem.* **282**: 14437–14446.

- Larson, T. R., T. Edgell, J. Byrne, K. Dehesh, and I. A. Graham. 2002. Acyl CoA profiles of transgenic plants that accumulate medium-chain fatty acids indicate inefficient storage lipid synthesis in developing oilseeds. *Plant J.* **32**: 519–527.
- Larson, T. R., and I. A. Graham. 2001. Technical advance: a novel technique for the sensitive quantification of acyl CoA esters from plant tissues. *Plant J.* **25**: 115–125.
- Sayanova, O., R. Haslam, M. Venegas Caleron, and J. A. Napier. 2007. Cloning and characterization of unusual fatty acid desaturases from *Anemone leveillei*: identification of an acyl-coenzyme A C20 Delta5-desaturase responsible for the synthesis of sciadonic acid. *Plant Physiol.* **144**: 455–467.
- Nagamori, I., K. Yomogida, P. D. Adams, P. Sassone-Corsi, and H. Nojima. 2006. Transcription factors, cAMP-responsive element modulator (CREM) and Tisp40, act in concert in postmeiotic transcriptional regulation. *J. Biol. Chem.* **281**: 15073–15081.
- Kai, M., M. Irie, T. Okutsu, K. Inoue, N. Ogonuki, H. Miki, M. Yokoyama, R. Migishima, K. Muguruma, H. Fujimura, et al. 2004. The novel dominant mutation *Dspd* leads to a severe spermiogenesis defect in mice. *Biol. Reprod.* **70**: 1213–1221.
- Vitale, M. L., C. D. Akpovi, and R. M. Pelletier. 2009. Cortactin/tyrosine-phosphorylated cortactin interaction with connexin 43 in mouse seminiferous tubules. *Microssc. Res. Tech.* **72**: 856–867.
- Stoffel, W., B. Holz, B. Jenke, E. Binczek, R. H. Gunter, C. Kiss, I. Karakesisoglou, M. Thevis, A. A. Weber, S. Arnhold, et al. 2008. Delta6-desaturase (FADS2) deficiency unveils the role of omega3- and omega6-polyunsaturated fatty acids. *EMBO J.* **27**: 2281–2292.
- Stroud, C. K., T. Y. Nara, M. Roqueta-Rivera, E. C. Radlowski, P. Lawrence, Y. Zhang, B. H. Cho, M. Segre, R. A. Hess, J. T. Brenna, W. M. Haschek, and M. T. Nakamura. 2009. Disruption of FADS2 gene in mice impairs male reproduction and causes dermal and intestinal ulceration. *J. Lipid Res.* **50**: 1870–80.
- Roqueta-Rivera, M., C. K. Stroud, W. M. Haschek, S. J. Akare, M. Segre, R. S. Brush, M. P. Agbaga, R. E. Anderson, R. A. Hess, and M. T. Nakamura. 2010. Docosahexaenoic acid supplementation fully restores fertility and spermatogenesis in male delta-6 desaturase knockout mice. *J. Lipid Res.* **51**: 360–7.
- Wang, Y., L. Wang, H. Jordanov, E. A. Swietlicki, Q. Zheng, S. Jiang, Y. Tang, M. S. Levin, and D. C. Rubin. 2006. Epimorphin^{-/-} mice have increased intestinal growth, decreased susceptibility to dextran sodium sulfate colitis, and impaired spermatogenesis. *J. Clin. Invest.* **116**: 1535–1546.
- Akiyama, K., S. Akimaru, Y. Asano, M. Khalaj, C. Kiyosu, A. A. Masoudi, S. Takahashi, K. Katayama, T. Tsuji, J. Noguchi, et al. 2008. A new ENU-induced mutant mouse with defective spermatogenesis caused by a nonsense mutation of the syntaxin 2/epimorphin (*Stx2/Epim*) gene. *J. Reprod. Dev.* **54**: 122–128.
- Low, S. H., X. Li, M. Miura, N. Kudo, B. Quinones, and T. Weimbs. 2003. Syntaxin 2 and endobrevin are required for the terminal step of cytokinesis in mammalian cells. *Dev. Cell.* **4**: 753–759.
- Szafer-Glusman, E., M. G. Giansanti, R. Nishihama, B. Bolival, J. Pringle, M. Gatti, and M. T. Fuller. 2008. A role for very-long-chain fatty acids in furrow ingression during cytokinesis in *Drosophila* spermatocytes. *Curr. Biol.* **18**: 1426–1431.
- Aveldano, M. I., and H. Sprecher. 1987. Very long chain (C24 to C36) polyenoic fatty acids of the n-3 and n-6 series in dipolyunsaturated phosphatidylcholines from bovine retina. *J. Biol. Chem.* **262**: 1180–1186.
- Rabionet, M., A. C. van der Spoel, C. C. Chuang, B. von Tumpling-Radosta, M. Litjens, D. Bouwmeester, C. C. Hellbusch, C. Korner, H. Wiegandt, K. Gorgas, et al. 2008. Male germ cells require polyenoic sphingolipids with complex glycosylation for completion of meiosis: a link to ceramide synthase-3. *J. Biol. Chem.* **283**: 13357–13369.
- Furland, N. E., G. M. Oresti, S. S. Antollini, A. Venturino, E. N. Maldonado, and M. I. Aveldano. 2007. Very long-chain polyunsaturated fatty acids are the major acyl groups of sphingomyelins and ceramides in the head of mammalian spermatozoa. *J. Biol. Chem.* **282**: 18151–18161.
- Kierszenbaum, A. L., E. Rivkin, and L. L. Tres. 2007. Molecular biology of sperm head shaping. *Soc. Reprod. Fertil. Suppl.* **65**: 33–43.
- Moon, Y. A., R. E. Hammer, and J. D. Horton. 2009. Deletion of ELOVL5 leads to fatty liver through activation of SREBP-1c in mice. *J. Lipid Res.* **50**: 412–423.

29. Edwards, A. O., L. A. Donoso, and R. Ritter 3rd. 2001. A novel gene for autosomal dominant Stargardt-like macular dystrophy with homology to the SUR4 protein family. *Invest. Ophthalmol. Vis. Sci.* **42**: 2652–2663.
30. Zhang, K., M. Kniazeva, M. Han, W. Li, Z. Yu, Z. Yang, Y. Li, M. L. Metzker, R. Allikmets, D. J. Zack, et al. 2001. A 5-bp deletion in ELOVL4 is associated with two related forms of autosomal dominant macular dystrophy. *Nat. Genet.* **27**: 89–93.
31. Karan, G., Z. Yang, K. Howes, Y. Zhao, Y. Chen, D. J. Cameron, Y. Lin, E. Pearson, and K. Zhang. 2005. Loss of ER retention and sequestration of the wild-type ELOVL4 by Stargardt disease dominant negative mutants. *Mol. Vis.* **11**: 657–664.
32. Grayson, C., and R. S. Molday. 2005. Dominant negative mechanism underlies autosomal dominant Stargardt-like macular dystrophy linked to mutations in ELOVL4. *J. Biol. Chem.* **280**: 32521–32530.
33. Bernstein, P. S., J. Tammur, N. Singh, A. Hutchinson, M. Dixon, C. M. Pappas, N. A. Zabriskie, K. Zhang, K. Petrukhin, M. Leppert, et al. 2001. Diverse macular dystrophy phenotype caused by a novel complex mutation in the ELOVL4 gene. *Invest. Ophthalmol. Vis. Sci.* **42**: 3331–3336.
34. Tikhonenko, M., T. A. Lydic, Y. Wang, W. Chen, M. Opreanu, A. Sochacki, K. M. McSorley, R. L. Renis, T. Kern, D. B. Jump, et al. 2009. Remodeling of retinal fatty acids in an animal model of diabetes: a decrease in long chain polyunsaturated fatty acids is associated with a decrease in fatty acid elongases Elovl2 and Elovl4. *Diabetes*. **59**:219–27.
35. Cameron, D. J., Z. Tong, Z. Yang, J. Kaminoh, S. Kamiyah, H. Chen, J. Zeng, Y. Chen, L. Luo, and K. Zhang. 2007. Essential role of Elovl4 in very long chain fatty acid synthesis, skin permeability barrier function, and neonatal survival. *Int. J. Biol. Sci.* **3**: 111–119.
36. Tanaka, T., J. Shen, G. R. Abecasis, A. Kisiailiou, J. M. Ordovas, J. M. Guralnik, A. Singleton, S. Bandinelli, A. Cherubini, D. Arnett, et al. 2009. Genome-wide association study of plasma polyunsaturated fatty acids in the InCHIANTI study. *PLoS Genet.* **5**: e1000338.
37. Illig, T., C. Gieger, G. Zhai, W. Romisch-Margl, R. Wang-Sattler, C. Prehn, E. Altmaier, G. Kastenmuller, B. S. Kato, H. W. Mewes, et al. 2010. A genome-wide perspective of genetic variation in human metabolism. *Nat. Genet.* **42**: 137–141.